

Journal of Materials Chemistry A

Accepted Manuscript

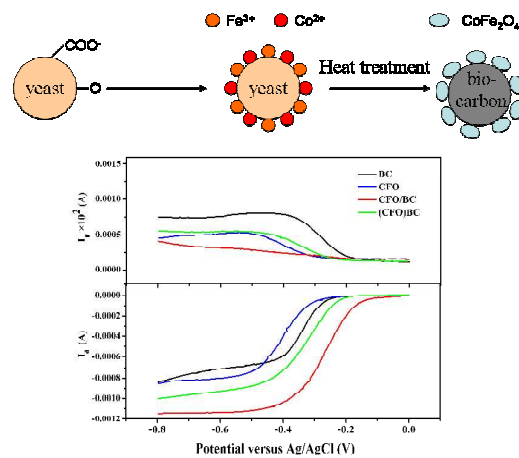


This is an *Accepted Manuscript*, which has been through the Royal Society of Chemistry peer review process and has been accepted for publication.

Accepted Manuscripts are published online shortly after acceptance, before technical editing, formatting and proof reading. Using this free service, authors can make their results available to the community, in citable form, before we publish the edited article. We will replace this *Accepted Manuscript* with the edited and formatted *Advance Article* as soon as it is available.

You can find more information about *Accepted Manuscripts* in the [Information for Authors](#).

Please note that technical editing may introduce minor changes to the text and/or graphics, which may alter content. The journal's standard [Terms & Conditions](#) and the [Ethical guidelines](#) still apply. In no event shall the Royal Society of Chemistry be held responsible for any errors or omissions in this *Accepted Manuscript* or any consequences arising from the use of any information it contains.



The CoFe₂O₄/biocarbon (CFO/BC) nanocomposites have been synthesized via a facile biosynthesis method using yeast cells as carbon sources and structural templates. The high electrocatalytic activity and durability of CFO/BC nanocomposites are mainly attributed to the strong coupling between CoFe₂O₄ nanoparticles and biocarbon as well as the hierarchical structure of CFO/BC.

Cite this: DOI: 10.1039/c0xx00000x

ARTICLE TYPE

www.rsc.org/xxxxxx

A Facile Synthesis of CoFe₂O₄/Biocarbon Nanocomposites as Efficient Bi-functional Electrocatalysts for Oxygen Reduction and Oxygen Evolution Reaction

Shanshan Liu^{a,b}, Weiyong Bian^b, Zhenrong Yang^b, Jinghua Tian^b, Chao Jin^b, Ming Shen^c, Zhufa Zhou^{*a},
5 and Ruizhi Yang^{*b}

Received (in XXX, XXX) Xth XXXXXXXXX 20XX, Accepted Xth XXXXXXXXX 20XX

DOI: 10.1039/b000000x

Efficient electrocatalysts for the oxygen reduction reaction (ORR) and oxygen evolution reaction (OER) are crucial for improving the performance of metal–air batteries. In this study, CoFe₂O₄/biocarbon (CFO/BC) nanocomposites have been synthesized via a facile biosynthesis method by using yeast cells as carbon sources and structural templates. The as-prepared CFO/BC nanocomposites possess hierarchical structure with high surface area (79.84 m² g⁻¹). The rotating ring-disk electrode (RRDE) and rotating disk electrode (RDE) measurements have revealed that CFO/BC nanocomposites exhibit excellent catalytic activity for both the ORR and OER. The onset potential of CFO/BC for ORR is -0.14 V (vs. Ag/AgCl), which is higher than that of CoFe₂O₄ (-0.29 V) and that of biocarbon (-0.25 V), respectively. Meanwhile, the CFO/BC nanocomposites show much higher activity for OER as compared to CoFe₂O₄ and biocarbon. The chronoamperometric tests show that CFO/BC catalyst shows high durability for both the ORR and OER, outperforming the commercial Pt/C(20 wt.% Pt on Vulcan XC-72, Johnson Matthey). The high electrocatalytic activity and durability of CFO/BC nanocomposite are mainly attributed to the strong coupling between CoFe₂O₄ nanoparticles and biocarbon as well as the hierarchical structure of CFO/BC.

1. Introduction

To mitigate the impacts of global warming and the depletion of fossil fuel on the whole world, the development of renewable energy production and storage system with high energy and power density is highly desirable. Rechargeable metal-air batteries have attracted much attention for their application as next generation power sources for portable electronic devices and especially electric vehicles, due to their extremely high energy density, low cost and environmental benignity.¹⁻⁴ Recent studies have shown that the performance of the rechargeable metal-air battery is mainly limited by the sluggish kinetics of the oxygen reduction reaction (ORR) and oxygen evolution reaction (OER) at the cathode.⁵ Traditionally, platinum-based materials are used as the catalysts to speed up the reactions, but they are expensive and scarce.^{6,7} Substantial efforts have been dedicated to searching for non-noble metal catalysts as a substitute for the noble metals. As a result, various catalysts have been explored, such as Co₃O₄,⁸ MnO₂,⁹ Fe₂O₃,¹⁰ graphene/Mn₃O₄ hybrid,¹¹ carbon-supported cobalt polypyrrole,¹² heteroatom-doped carbon.¹³ These materials have been demonstrated as promising electrocatalysts for the cathode of metal-air batteries. Especially, spinel oxides have been paid more and more attention due to their high catalytic activities toward ORR and OER. Du et

al.¹⁴ have reported that one-dimensional CaMn₂O₄ prepared by a solvothermal method exhibited considerable catalytic activities and enabled an apparent quasi-four-electron transfer in the ORR. High electrocatalytic activities of MnCo₂O₄ for ORR in alkaline solution have also been reported by Liang et al.¹⁵ Recently, Sun et al.¹⁶ reported that NiCo₂O₄ nanorods used as air electrode for lithium-air battery showed low charge over-potential, high discharge capacity and high-rate capability. Although cobaltite spinel oxides have been widely investigated as electrocatalysts, the electrocatalytic activities of CoFe₂O₄ for the ORR and OER are still seldom reported.

Due to the poor electron conductivity of spinel oxides, they are usually attached to or supported on a conducting surface (like carbon) to assure fast electron transport. Moreover, the structure of supports is crucial for the mass transfer in the triple phase (solid-liquid-gas) regions required for oxygen reduction and oxygen evolution.¹⁷⁻¹⁹ Many different nanostructured carbon supports including carbon nanotubes,²⁰ graphene,²¹ and carbon fibers²² have been reported to improve the performance of the air electrode, which are ascribed to the improved mass transfer facilitated by their unique structure.

In this report, we demonstrate a bio-synthesis approach for preparing CoFe₂O₄ /biocarbon (CFO/BC) nanocomposites. Low cost yeast cells were used as biocarbon sources as well as structural templates. On the one hand, CFO/BC nanocomposites

can be synthesized via a biomineralization process in an environmental friendly system with yeast cells as biocarbon sources. On the other hand, the phase, size and morphology of the composites can be easily controlled by tuning the biomineralization conditions with yeast cells as structural templates. Moreover, biocarbon carbonized from yeast cells is actually N and P doped carbon, which is beneficial for the ORR.²³⁻²⁶ The electrocatalytic activities of CFO/BC nanocomposites for ORR and OER in alkaline media have been studied by using rotating ring-disk electrode (RRDE) and rotating disk electrode (RDE) techniques. The CFO/BC nanocomposites showed high electrocatalytic activities for both the ORR and OER with superior long-term stability in alkaline media.

2. Experimental

2.1 Sample Preparation

The reagents used in this work were $\text{Co}(\text{NO}_3)_2 \cdot 6\text{H}_2\text{O}$ (99%, Sinopharm Chemical Reagent Co., Ltd.), $\text{Fe}(\text{NO}_3)_3 \cdot 9\text{H}_2\text{O}$ (99.5%, Sinopharm Chemical Reagent Co., Ltd), NH_4OH (vol.%=27%, Tianjin BodiChemical Co., Ltd.), and yeast (Instant dry yeast, Angel Yeast Co., Ltd.). Ultrapure water was used during the synthesis.

The CFO/BC nanocomposites were prepared using the biotemplate and chemical precipitation route as described below. Quantitative instant dry yeast (1g) was cultivated in glucose aqueous solution (250 mL) at 30 °C. After 30 min of stirring, the purified yeast cells were obtained by centrifugation and washing with ultrapure water. Then obtained yeast cells were dissolved in deionized water (100 mL) to form a uniform bioemulsion. In the synthesis of the nanocomposite catalyst, the stoichiometric $\text{Co}(\text{NO}_3)_2$ (0.0015 mol) and $\text{Fe}(\text{NO}_3)_3$ (0.003 mol) were added to the solution while stirring for 2 h at ambient temperature. NH_4OH was used as the precipitation reagent and added dropwisely under vigorous stirring for 4 h. After that, the suspension was transferred to a lyophilizer and dried at -47 °C for 24 h. The powder was sintered in a quartz tube with flowing N_2 at 400 °C for 2 h for biomineralization of yeast cells and crystallization of CoFe_2O_4 . The final product was black powder of CoFe_2O_4 /biocarbon being marked as CFO/BC.

Biocarbon was also prepared with same procedure without adding any metal salts and NH_4OH . The obtained biocarbon was denoted as BC. Pure CoFe_2O_4 was also prepared in the absence of yeast cells, and the final product was denoted as CFO.

2.2 Physical characterization

The crystal structure of the samples were characterized by powder X-ray diffraction (XRD) using a Bede D1 X-ray diffractometer with $\text{Cu-K}\alpha$ radiation (UK, Bede Scientific Ltd.; operated at 40 kV, 45mA; $\lambda = 0.15418$ nm), the diffraction angle ranging from 10° to 80° with a step of 0.02° and a rate of 2°min⁻¹.

Scanning electron microscopy (SEM) images of the samples were obtained on a Quanta 200 scanning electron microscope (Hitachi) with an accelerating voltage of 15 kV.

The microstructure of the samples was characterized by a transmission electron microscope (TEM, HT7700, Japan) operating at 200 kV.

The specific surface area and the pore structure of the samples were analyzed by adsorption/desorption measurements of

nitrogen at 77 K (TriStar II 3020). Surface area was calculated by Brunauer-Emmett-Teller (BET) method. Pore size distributions were calculated using Barrett-Joyner-Halenda (BJH) method.

Surface analysis of the samples was carried out with a X-ray photoelectron spectroscopy spectrometer (XPS, VG ESCALAB MKII) using a $\text{Al K}\alpha$ source.

2.3 Electrochemical measurements

The electrocatalytic activities of the samples were conducted with the rotating ring-disk electrode (RRDE) technique using a Pine electrochemical system (AFMSRX rotator, and AFCBP1 bipotentiostat). The RRDE electrode consisted of a catalyst-coated GC disk (5 mm diameter, 0.196 cm² of geometric surface area) surrounded by a Pt ring (0.125 cm² of geometric surface area). A standard three-electrode electrochemical cell was used. An Ag/AgCl (3 M Cl^-) electrode and Pt-foil were used as the reference and counter electrode, respectively. Inks of the catalyst were prepared by mixing 5 mg of catalyst, 5 mg of acetylene black, 48 μL of Nafion solution (5 wt.%, Aldrich) and 350 μL of ethanol, followed by ultrasonication for 40 minutes. Seven μL of the ink was pipetted onto a GC disk resulting in a catalyst loading of 503 $\mu\text{g}/\text{cm}^2$. The same catalyst loading was used for commercial Pt/C (20wt % Pt on Vulcan XC-72, Johnson Matthey) for comparison. 0.1 M KOH aqueous solution was used as the electrolyte. The electrolyte was purged with either high-purity Ar or O_2 for at least 30 mins before each measurement. The samples on the GC disks were first electrochemically cleaned by sweeping the potential in the range between -0.9 and 0 V (vs. Ag/AgCl) at 50 mV s⁻¹ in an N_2 -saturated 0.1 M KOH solution until steady state cyclic voltammograms (CV) were obtained. For each catalyst tested, a CV with the same scanning rate as that for ORR/OER was first collected to determine the non-Faradaic current.

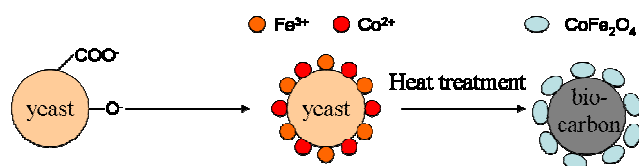
For the ORR test, measurements during oxygen reduction were performed in O_2 -saturated 0.1 M KOH by sweeping the potential from 0 V cathodically to -0.8 V at 5 mV s⁻¹ with the electrode rotated at 400, 900, 1600 and 2500 rpm and O_2 gas purged into the solution at a flow rate of 25 sccm through a 2 mm fritted tube (Ace Glass). The current density was obtained from the ORR data and then normalized by the geometric surface area. The Koutecky-Levich (K-L) plot relates the current density (J) to the angular velocity (ω) to calculate the number of electron transferred (n) during the ORR process according to K-L equation:²⁷

$$\frac{1}{J} = \frac{1}{J_L} + \frac{1}{J_K} = \frac{1}{B\omega^{1/2}} + \frac{1}{J_K} \quad (1)$$

$$B = 0.62nFC_{\text{O}_2}D_{\text{O}_2}^{2/3}\nu^{-1/6} \quad (2)$$

in which J corresponds to the measured current density, J_K and J_L are the kinetic and diffusion-limiting current densities, respectively, F is the Faraday constant, C_{O_2} is the saturated concentration of O_2 in electrolyte, D_{O_2} is the diffusion coefficient of O_2 , and ν is the kinetic viscosity of the solution.

For all the RRDE measurements, the disk electrode was scanned at a rate of 5 mV s⁻¹, and the ring potential was held at 0.5 V (vs. Ag/AgCl). The percentage of peroxide species with respect to the total oxygen reduction products and the electron number transferred during the ORR process can be determined by the following equations:²⁸



Scheme 1 Schematic illustration of the synthesis of CFO/BC.

$$HO_2^- = 200 \frac{I_r / N}{I_d + I_r / N} \quad (3)$$

$$n = 4 \frac{I_d}{I_d + I_r / N} \quad (4)$$

where I_d is disk current, I_r is ring current, and N is current collection efficiency of the Pt ring ($N=0.22$).

For the OER test, only rotating-disk electrode (RDE) was used, the working electrode was scanned from 0 to 1.0 V (vs. Ag/AgCl) at a scan rate of 5 mV s⁻¹ in a N₂-saturated electrolyte with the electrode rotated at 1600 rpm.

3. Results and discussion

Scheme 1 shows the preparation of CFO/BC nanocomposites with yeast cells as carbon sources and structural templates. After adding Co²⁺ and Fe³⁺ ions to the purified yeast cell solution, Co²⁺ and Fe³⁺ combine with the negative groups OH⁻ and COO⁻ on the surface of the yeast cells by electrostatic interaction. Thus CoFe₂O₄ is formed and self-assembled on the surface of the yeast cells via a biomineralization. After heat-treatment in Ar atmosphere, CoFe₂O₄/biocarbon (i.e. CFO/BC) nanocomposites are obtained.

Fig. 1 shows the X-ray diffraction (XRD) pattern of the as-obtained CFO/BC nanocomposites. The XRD pattern of CFO and BC are also included for comparison. The characteristic peaks of the CFO/BC nanocomposites and pure CFO nanoparticles can be indexed as cubic spinel CoFe₂O₄ nanocrystals (PDF#22-1086). The broad peak at around 23° corresponds to the (002) carbon phase of the BC, indicates the formation of amorphous carbon.²⁹ The average crystallite size of the CFO particles in CFO/BC nanocomposites and in pure CFO are estimated to be 11.5 nm and 33.0 nm, respectively, by the Scherrer formula.³⁰ The small particle size of CFO nanoparticles in CFO/BC nanocomposites is due to the dispersing effect of biocarbon support in preventing the CFO nanoparticles from aggregation.

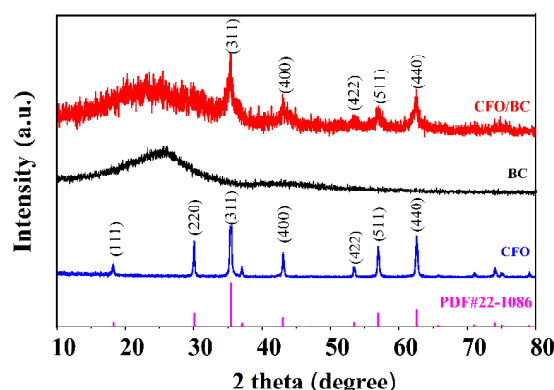


Fig. 1 XRD patterns of the synthesized CFO, BC and CFO/BC.

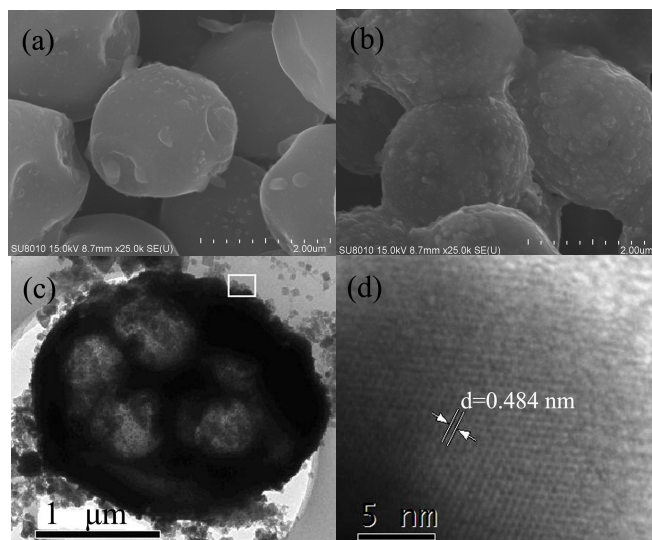


Fig. 2 SEM image of BC (a) and CFO/BC (b); (c) TEM image of CFO/BC; (d) HRTEM image of CFO/BC in the corresponding region of (c).

The morphology and structure of the CFO/BC was investigated by scanning electron microscopy (SEM) and transmission electron microscopy (TEM). Smooth spherical particles of BC with an average diameter of 1-2 μm are shown in Fig. 2a, which retains the spherical morphology of the live yeast cells as shown in Fig. S1. The surface of CFO/BC becomes rough due to the deposition of CFO on the surface of biocarbon spheres as shown in Fig. 2b.³¹ The TEM image (Fig.2c) clearly shows the dispersion of CFO nanoparticles on the surface of carbon spheres. Moreover, the macropores with a diameter of about 500 nm in the biocarbon network can be clearly observed. The crystal structure of the CFO nanoparticles on biocarbon was revealed by high-resolution TEM. The measured d spacing value of 0.484 nm is assigned to the (111) plane of CFO. The thermogravimetric analysis (TGA) of the sample in air was carried out on a TG/DTA7300 analyzer. The prepared CFO/BC was heated from room temperature to 800 °C with a heating rate of 10 °C min⁻¹. As shown in Fig.S3, about 39.2% weight loss is observed as the temperature is increased to 800 °C. The weight-loss is attributed to the burn-off of biocarbon in the CFO/BC. Therefore the actual loading of CoFe₂O₄ in CFO/BC electrocatalysts is 70.8%.

Fig. 3 shows the N₂ sorption isotherm and the pore size distribution.

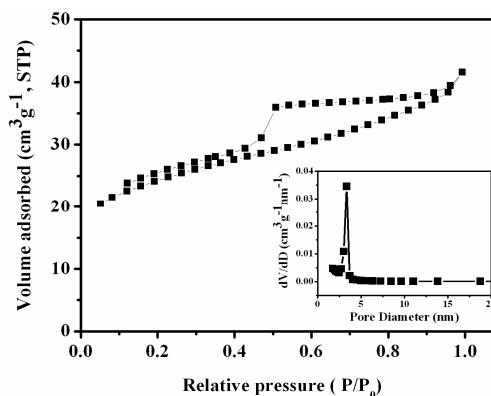
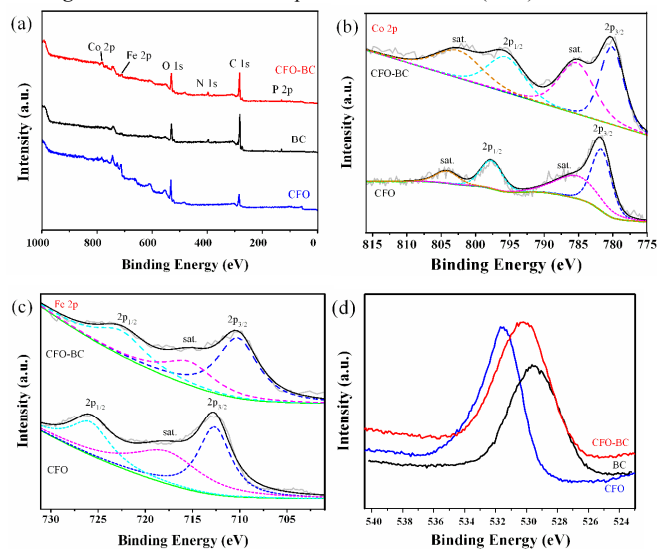
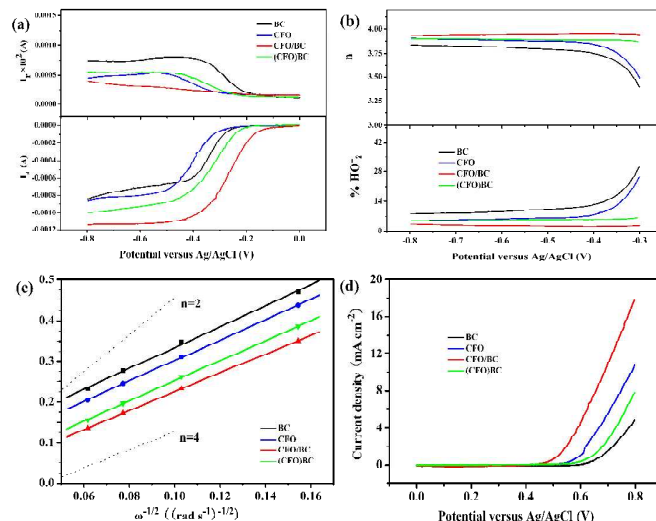


Fig. 3 BET surface area and pore size distribution (inset) of CFO/BC**Fig. 4** (a) XPS survey scan for CFO, BC and CFO/BC; (b) XPS spectra for the Co 2p of CFO and CFO/BC; (c) XPS spectra for the Fe 2p of CFO and CFO/BC; (d) XPS spectra for the O 1s of CFO and CFO/BC.

bution of CFO/BC. The N_2 -adsorption isotherm of the CFO/BC exhibits typeIV isotherm, indicating the mesoporosity in the sample. The mesopores with a narrow pore size distribution and an average diameter of 3.34 nm can be seen from the inset of Fig. 3. The CFO/BC displays a BET specific surface area of $79.84 \text{ m}^2 \text{ g}^{-1}$. The mesopores along with the macropores endow the sample a hierarchical structure. This structure allows O_2 and electrolyte to penetrate into the spheres easily and benefits the mass transfer.

To obtain the cation oxidation state and the chemical composition of the CFO/BC, X-ray photoelectron spectroscopy (XPS) measurements were performed. The XPS survey spectra in Fig. 4a shows the Co 2p, Fe 2p, O 1s and C 1s peaks in both CFO and CFO/BC. The N 1s peak at 403.3 eV and P 2p peak at 136 eV are found in the BC and CFO/BC, which come from the precursor yeast cells.

The de-convolution of the Co 2p peak in CFO and CFO/BC shows four peaks (Fig. 4b). In CFO sample, the peaks at a binding energy of 781.8 and 797.7 eV are from Co $2p_{3/2}$ and Co $2p_{1/2}$, respectively.²⁸⁻³⁰ The satellite peaks at around 785.5 and 804.3 eV are two shake-up type peaks of Co at the high binding energy side of the Co $2p_{3/2}$ and Co $2p_{1/2}$ edge. These indicate the presence of Co^{2+} in the sample. As compared with the binding energy of Co 2p in CFO, there is a shift of 1.6 eV for Co $2p_{3/2}$ and 1.9 eV for Co $2p_{1/2}$, respectively, in CFO/BC towards lower binding energy. The Fe 2p spectra are fitted into three peaks (Fig. 4c). The peaks at 712.6 eV and 725.4 eV are signed to Fe $2p_{3/2}$ and Fe $2p_{1/2}$, respectively.³²⁻³⁴ The peak at 717.9 eV is a satellite peak. These suggest the presence of Fe^{3+} cations in the sample. There is a more obvious shift of 2.4 eV for Fe $2p_{3/2}$ and 2.9 eV for Fe $2p_{1/2}$ in CFO/BC towards lower binding energy as compared with the binding energy of Fe 2p in CFO. The shift of the binding energy in Co 2p and Fe 2p reveals the strong coupling between CFO and BC. As shown in Fig. 4d, the O 1s spectra in CFO shows a peak at 531.6 eV, corresponding to the lattice oxygen in the Co/Fe-O framework.³²⁻³⁶ The binding energy of O 1s in BC at 529.5 eV is

**Fig. 5** (a) Linear sweeping voltammograms (LSVs) on rotating ring-disk electrode for CFO, BC, CFO/BC hybrid and (CFO)BC (CFO/BC etched by 3 M HCl) in O_2 -saturated 0.1 M KOH at a rotating speed of 1600 rpm. The disk potential was scanned at 10 mV s^{-1} and the ring potential was fixed at 0.5 V (vs. Ag/AgCl). (b) Calculated electron transfer number n and peroxide percentage at various potentials based on the corresponding RRDE data in (a). (c) Koutecky-Levich plots based on ORR polarization curves in (a) at -0.6 V. (d) LSVs for the OER on CFO, BC, (CFO)BC and CFO/BC in N_2 -saturated 0.1 M KOH with a sweeping rate of 10 mV s^{-1} and a rotating speed of 1600 rpm

assigned to $-COOH$ and/or $-OH$ chemical bindings. The binding energy of O 1s in CFO/BC is 530.2 eV, which is between that in CFO and BC, indicating the formation of interfacial M-O-C in CFO/BC. This indicates that the coupling between CFO and BC occurs through the $-COOH$ and $-OH$ functional groups of the yeast cells.

To assess the ORR activity of the samples, the polarization curves for the ORR on pure CFO nanoparticles, BC and CFO/BC nanocomposites in O_2 saturated 0.1 M KOH solutions at a rotation rate of 1600 rpm are shown in Fig. 5a. The onset potentials of CFO and BC are about -0.29 V and -0.25 V, respectively. In contrast, CFO/BC shows a much higher onset potential of -0.14 V. This indicates that the ORR activity of CFO/BC is higher than that of CFO and BC. The formation of peroxide species (HO_2^-) and electron number transferred during the ORR process were monitored with RRDE measurements (Fig. 5a and b). The measured HO_2^- yield on the catalysts decreases as follows: $BC > CFO > (CFO)BC > CFO/BC$, and the corresponding electron number transferred during the ORR reaction decreases in the reverse order. The measured HO_2^- yield is 9-30% for BC and 5-24% for CFO, 5-7% for (CFO)BC and it significantly decreases to below 3.2% for CFO/BC hybrid catalyst over the potential range of -0.80 to -0.30 V. The electron transfer number on BC, CFO, (CFO)BC and CFO/BC hybrid are 3.40-3.83, 3.51-3.92, 3.86-3.90 and 3.93-3.95, respectively (Fig. 5b). The evidently lower HO_2^- production and higher electron transfer number on CFO/BC as compared with those on CFO and BC suggests the improved ORR pathway on CFO/BC. When CFO/BC was etched by HCl, $CoFe_2O_4$ nanocrystals were removed and more catalytic active sites were left on the surface,

so the catalytic performance of (CFO)BC was enhanced as compared with the pure BC. In addition, the CFO/BC shows much better ORR and OER catalytic activities than Co/BC (only $\text{Co}(\text{NO}_3)_2$ was added into the yeast emulsion and the other experiment conditions were the same) and Fe/BC (only $\text{Fe}(\text{NO}_3)_3$ was added into the yeast emulsion and the other experiment conditions were the same), which clarify the important role of CoFe_2O_4 in the catalytic activity of the as-prepared composite material (see Fig.S4 and Fig.S5). Fig. 5c shows the corresponding Koutecky-Levich (K-L) plots at -0.6 V for BC, CFO, (CFO)BC and CFO/BC. These plots are linear, indicating the first-order dependence of the kinetics of ORR on the three samples. The electron transfer numbers on BC, CFO, (CFO)BC and CFO/BC sample are 3.56, 3.63, 3.70 and 3.95, respectively, which are consistent with the results obtained from Fig.3b. Note that the number of electron transferred on BC (3.40-3.83) is different from the classical 2-electron pathway on pure carbon reported elsewhere.³⁷⁻³⁹ The BC sample contains 6.29 at.% N and 2.62 at.% P as obtained from XPS analysis, which derive from the yeast cells. So the synthesized BC is actually a carbon doped with N and P. Studies have shown that heteroatom N and P doping can improve the activity of carbon for ORR.⁴⁰⁻⁴² This can explain why the as-obtained BC in this study shows higher activity than the common carbon. However, no shifts in the binding energy of N1s and P2p have been observed in CFO/BC as compared to BC, indicating no interaction between CFO and N or P in BC. However, as analyzed above (Fig.4), there is strong coupling between CFO and BC via the -COOH and -OH functional groups of the yeast cells. The high ORR activity and improved ORR pathway on CFO/BC are mainly attributed to the strong coupling between CFO and BC. Meanwhile the hierarchical structure of CFO/BC allows the easy access and transport of O_2 and electrolyte, increasing the triple-phase contact area of the reaction.

Fig. 5d shows the OER activities of the electrocatalysts. The CFO/BC hybrid exhibits an onset potential of 0.46 V, which is 90 mV lower than that of CoFe_2O_4 and 160 mV lower than that of BC. The current density of CFO/BC at 0.8 V reaches 17.7 mA cm^{-2} , which is much higher than that of CoFe_2O_4 (10.6 mA cm^{-2}) and BC (4.7 mA cm^{-2}). These results clearly show that CFO/BC hybrid possess both high ORR activity and OER activity.

The stabilities of CFO/BC catalysts for the ORR and OER were examined with the chronoamperometric method and were compared with those of commercial Pt/C (20 wt.%). As shown in Fig. 6, the ORR current density of CFO/BC decreases 15.1% at a constant potential of -0.35 V over 43000 s of continuous operation. While the ORR current on commercial Pt/C decreases 52.4% after 43000 s. The OER stability of CFO/BC is more obvious. Comparing to a decrease of 69.8% for Pt/C, only a decrease of 1.4% in the OER current density for CFO/BC was observed at the potential of 0.80 V after 43000 s. The results reveal that the CFO/BC hybrid is quite stable for both the ORR and OER, which most likely results from the coupling between CoFe_2O_4 and biocarbon.

4. Conclusions

In conclusion, CFO/BC nanocomposites were synthesized via a facile and environmental friendly biosynthesis approach. The

CFO/BC nanocomposites exhibit highly efficient electrocatalytic activities for both ORR and OER. Moreover, the CFO/BC nanocomposites show excellent stability for both ORR and OER, outperforming commercial Pt/C (20 wt.%) in alkaline media. In view of the low cost of yeast cells and CoFe_2O_4 , CFO/BC nanocomposites could be promising non-precious electrocatalysts for metal-air batteries.

Acknowledgements

This work was supported by National Natural Science Foundation of China (Grant Nos. 51272167 and 21206101), Priority Academic Program Development (PAPD) of Jiangsu Higher Education Institutions and Natural Science Foundation of the Higher Education Institutions of Jiangsu Province, China(12KJB430010).

Notes and references

- ^a College of Chemistry, Chemical Engineering and Materials Science, Soochow University, Suzhou 215006, China.
- ^b College of Physical, Optoelectronics and Energy & Collaborative Innovation Center of Suzhou Nano Science and Technology, Soochow University, Suzhou 215006, China. Tel: +86 512 65221519; E-mail: yangrz@suda.edu.cn, zfzhou@suda.edu.cn
- ^c Huasheng Chemical Corporation, Zhangjiagang, Jiangsu 215635, China
- 1 K. M. Abraham, Z. Jiang, *J. Electrochem. Soc.* 1996, **143**, 1.
- 2 P. G. Bruce, S. A. Freunberger, L. J. Hardwick, J.-M. Tarascon, *Nat. Mater.* 2012, **11**, 19.
- 3 Y. C. Lu, H. A. Gasteiger, Y. Shao-Horn, *J. Am. Chem. Soc.* 2011, **133**, 19048.
- 4 J. S. Lee, S. T. Kim, R. Cao, N. S. Choi, M. Liu, K. T. Lee, J. Cho, *Adv. Energy Mater.* 2011, **1**, 34.
- 5 J. Zhang, H. Z. Yang, J. Y. Fang, S. Z. Zou, *Nano Lett.* 2010, **10**, 638.
- 6 M. H. Shao, G. N. He, A. Peles, J. H. Odella, J. Zeng, D. Su, J. Tao, T. K. Yu, Y. M. Zhu, Y. N. Xia, *Chem. Commun.* 2013, **49**, 9030.
- 7 V. R. Stamenkovic, B. Fowler, B. S. Mun, G. F. Wang, P. N. Ross, C. A. Lucas, N. M. Markovic, *Science* 2007, **315**, 493.
- 8 J. A. Koza, Z. He, A. S. Miller, J. A. Switzer, *Chem. Mater.* 2012, **24**, 3567.
- 9 L. Jin, L. P. Xu, C. Morein, C. H. Chen, M. Lai, S. Dharmarathna, A. Doble, S. L. Suib, *Adv. Funct. Mater.* 2010, **20**, 3373.
- 10 W. Y. Zhang, Y. Zeng, C. Xu, H. T. Tan, W. L. Liu, J. X. Zhu, N. Xiao, H. H. Hng, J. Ma, H. E. Hoster, R. Yazami, Q. Y. Yan, *RSC Adv.* 2012, **2**, 8508.
- 11 J. S. Lee, T. M. Lee, H. K. Song, J. P. Cho, B. S. Kim, *Energy Environ. Sci.* 2011, **4**, 4148
- 12 K. Lee, L. Zhang, H. S. Lui, R. Hui, Z. Shi, J. J. Zhang, *Electrochim. Acta* 2009, **54**, 4704.

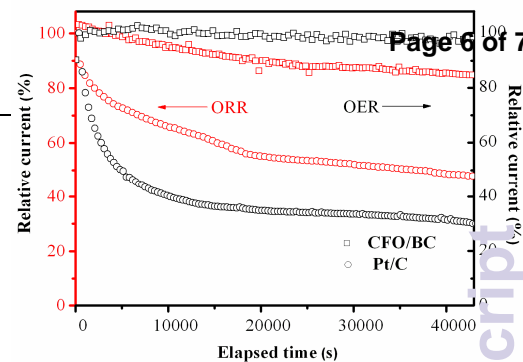


Fig. 6 Current-time (i-t) chronoamperometric responses for the ORR and the OER on synthesized $\text{CoFe}_2\text{O}_4/\text{BC}$ and commercial Pt/C in O_2 -saturated 0.1 M KOH at -0.35 V (vs. Ag/AgCl) for ORR and in N_2 -saturated 0.1 M KOH at 0.8 V for OER at a rotating speed of 1600 rpm.

- 13 J. L. Shui, N. K. Karan, M. Balasubramanian, S. Y. Li, D. J. Liu, *J. Am. Chem. Soc.* 2012, **134**, 16654.
- 14 J. Du, Y. D. Pan, T. R. Zhang, X. P. Han, F. Y. Cheng, J. Chen, *J. Mater. Chem.* 2012, **22**, 15812
- 5 15 Y. Y. Liang, H. L. Wang, J. G. Zhou, Y. G. Li, J. Wang, T. Regier, H. J. Dai, *J. Am. Chem. Soc.* 2012, **134**, 3517.
- 16 B. Sun, J. Q. Zhang, P. Munroe, H. J. Ahn, G. X. Wang, *Electrochem. Commun.* 2013, **31**, 88.
- 17 D. Zheng, H. S. Lee, X. Q. Yang, D. Y. Qu, *Electrochem. Commun.* 2013, **28**,
- 10 18 E. J. Yoo, H. S. Zhou, *ACS Nano* 2011, **5**, 3020.
- 19 S. S. Zhang, D. Foster, J. Read, *J. Power Sources* 2010, **195**, 1235.
- 20 Y. Yan, W. Zheng, L. Su, L. Mao, *Adv. Mater.* 2006, **18**, 2639.
- 21 J. Xiao, D. H. Mei, X. L. Li, W. Xu, D. Y. Wang, G. L. Graff, W. D. Bennett, Z. M. Nie, L. V. Saraf, I. A. Aksay, J. Liu, J. G. Zhang, *Nano Lett.* 2011, **11**, 5071.
- 22 R. R. Mitchell, B. M. Gallant, C. V. Thompson, Y. S. Horn, *Energy Environ. Sci.* 2011, **4**, 2952.
- 23 Y. J. Zhang, K. Fuqane, T. Mori, L. Niu, J. H. Ye, *J. Mater. Chem.* 2012, **22**, 6575.
- 20 24 N. Brun, S. A. Wohlgemuth, P. Osiceanu, M. M. Titirici, *Green Chem.* 2013, **15**, 2514.
- 25 Z. Schnepf, Y. J. Zhang, M. J. Hollamby, B. R. Pauw, M. Tanaka, Y. Matsushita, Y. Sakka, *J. Mater. Chem. A* 2013, **1**, 13576.
- 25 26 S. Yasuda, L. Yu, J. Kim, K. Murakoshi, *Chem. Commun.* 2013, **49**, 9627.
- 27 S. Treimer, A. Tang, D. C. Johnson, *Electroanal.* 2002, **14**, 165.
- 28 U. A. Paulus, T. J. Schmidt, H. A. Gasteiger, R. J. Behm, *J. Electroanal. Chem.* 2001, **495**, 134.
- 30 29 M. J. Noh, Y. J. Kwon, H. J. Lee, J. P. Cho, Y. J. Kim, M. G. Kim, *Chem. Mater.* 2005, **17**, 1926.
- 30 V. Radmilovic, H.A. Gasteiger, P.N.Ross Jr, *J. Catal.* 1995, **154**, 98.
- 31 X. Y. Du, W. He, X. D. Zhang, Y. Z. Yue, H. Liu, X. G. Zhang, D. D. Min, X. X. Ge, Y. Du, *J. Mater. Chem.* 2012, **22**, 5960.
- 35 32 H.L.Yuan, Y.Q. Wang, S. M. Zhou, L. S. Liu, X. L. Chen, S. Y. Lou, R.J. Yuan, Y.M. Hao, N. Li, *Nanoscale Res. Lett.* 2010, **5**, 1817.
- 33 G.B. Ji, S.L. Tang, S.K. Ren, F.M. Zhang, B.X. Gu, Y.W. Du, *J. Crystal Growth*, 2004, **270**, 156.
- 34 G.C. Allen, S.J. Harris, J.A. Jutson, J.M. Dyke, *Appl. Surf. Sci.* 1989, 40 **37**, 111.
- 35 Y. Sharma, N. Sharma, G.V. Subba Rao, B.V.R. Chowdari, *Solid State Ionics*, 2008, **179**, 587–597.
- 36 D. U. Lee, B. J. Kim and Z.W. Chen, *J. Mater. Chem. A*, 2013, **1**, 4754.
- 45 37 Y. M. Tan, C. F. Xu, G. X. Chen, X. L. Fang, N. F. Zheng, Q. J. Xie, *Adv. Funct. Mater.* 2012, **22**, 4584.
- 38 D-S. Yang, D. Bhattacharjya, S.Inamdar, J.Park, J-S. Yu, *J. Am. Chem. Soc.* 2012, **134**, 16127.
- 39 I-Y. Jeon, S.Zhang, L.Zhang, H-J. Choi, J-M. Seo, Z.H. Xia, L.M. Dai and J-B.Baek, *Adv. Mater.* 2013, **25**, 6138.
- 50 40 V. V. Strelko, N. T. Kartel, I. N. Dukhno, V. S. Kuts, R. B. Clarkson, B. M. Odintsov, *Surf. Sci.* 2004, **548**, 281.
- 41 D. S. Yu, Y.H. Xue, L.M.Dai, *J. Phys. Chem. Lett.* 2012, **3**, 2863.
- 42 J. Wu, Z. R. Yang, X. W. Li, Q. J. Sun, C. Jin, P. Strasser, R. Z. Yang, 55 *J. Mater. Chem. A*, 2013, **1**, 9889.